2.N

Nuclear Physics A277 (1977) 509–532; © *North-Holland Publishing Co., Amsterdam*

THE TIME-DEPENDENT SINGLE-PARTICLE METHOD FOR QUASIELASTIC HEAVY ION COLLISIONS†

G. BERTSCH

Physics Department, Michigan State University, East Lansing, Michigan 48824

and

R. SCHAEFFER

Centre d'Etude Nucléaire de Saclay, 91190 Gif-sur-Yvette, France

Received 26 May 1976

(Revised 7 September 1976)

Abstract: The dynamics of heavy ion collisions are modeled by solving the time-dependent Schrödinger equation for potential wells moving on classical trajectories. We find that particle transfer is much more likely than particle excitation in the same nucleus. This is at variance with most experiments, and the likely reason is that the model neglects collective enhancements of low excitations. It is found that the DWBA underestimates the weak transitions by large factors. For the moderately strong transitions where the magnitude is correct, the phases can be significantly different. The observed anomalous of $^{18}O(0^+ \rightarrow 2^+)$ correlates with the $d \rightarrow 1s$ phase obtained in this calculation. We achieve quantitative agreement with experiment for one- and two-particle transfer. For grazing collisions of ^{18}O and Sn at 100 MeV, the average energy loss is quite small, supporting the adiabatic picture of the single-particle degrees of freedom. For the earliest stages of the collision the single-particle dynamics can be easily characterized classically. However, at late stages of the collision a classical treatment does not give accurate velocities or transfer probabilities for the particles.

1. Introduction

There is a great interest in heavy ion collisions, with a wealth of experimental data now available. But there is as yet no theoretical framework to build an understanding of the data, especially at the higher energies where measurements are not of specific final states, but are averages over many final states. A promising method to appear is the time-dependent Hartree-Fock calculation [1]). This describes not only single-particle behavior but also collective oscillations at low energies. However, the method is technically difficult to apply to three-dimensional geometry and much of the physics may well be contained in the time-dependent Schrödinger equation, without demanding Hartree-Fock self-consistency. With this in mind we shall investigate the consequences of the time-dependent single-particle model where the single-particle Hamiltonian is solved for colliding potential wells. Calculations of heavy ion reactions in this spirit were first attempted by Breit *et al.* [2]). The approach of treating one aspect of the collision classically and another quantum mechanically has been exploited for inelastic as well as for transfer reactions by Broglia and Winther [3]). The difference is

† Research supported by the National Science Foundation.

that these authors treat the collective inelastic degrees of freedom of the nuclei, while we examine the single-particle behavior. With our treatment we hope to straddle the domains of peripheral collisions which excite individual final state and the closer collisions where strong damping is observed. We first discuss the formalism, then the technical method we used for integration and finally some results to compare with experiment.

2. Formulation

2.1. EQUATION OF MOTION

In principle, our starting point is the time-dependent Hartree-Fock theory. The wave function of the system is a Slater determinant based on the product wave function,

$$\psi = \prod \phi_i, \tag{1}$$

and the single-particle wave functions evolve in time according to

$$i \frac{\partial}{\partial t} \phi_i = \left(\frac{p^2}{2m} + V(\rho) \right) \phi_i, \tag{2}$$

where

$$\rho = \sum_i \phi_i^* \phi_i. \tag{3}$$

Our formulas will be expressed in units with $\hbar = 1$. Our actual calculations will use units of MeV, fm, and fm/c for time.

We shall assume that the self-consistent field $V(\rho)$ appearing in eq. (2) is adequately approximated by the sum of two potential wells moving on classical trajectories,

$$V(r) \approx V_A(r - R_A) + V_B(r - R_B), \tag{4}$$

where R_A and R_B are the centers of the two wells. Eq. (4) is not expected to be a good approximation for close collisions, so there will of course be some ambiguity in the determination of R_A and R_B. For peripheral collisions, R_A and R_B can be determined from the evolution of the wave functions in the two wells. Several prescriptions for the motion of R_A and R_B can be easily formulated. One prescription is to choose the time dependence to maximize the overlap with the ground-state wave functions referred to origins R_A and R_B. Another prescription is to choose the time dependence of the wells so as to conserve the total energy. This latter prescription can be formalized by explicitly introducing cluster coordinates and momenta into the Hamiltonian. This is done in the appendix.

In this paper we shall not study the self-consistent evolution of the coupled single-particle and ion trajectory equations, but merely examine qualitative and some quantitative aspects of the time-dependent single-particle behavior. To follow the evolution of a wave function which starts in nucleus A, it is useful to use a coordinate system centered at R_A. The initial wave function is the spherical eigenstate of the well,

$$h_A \phi_a^{(0)} = \varepsilon_a \phi_a^{(0)}. \tag{7}$$

Since the coordinate system is accelerating, the time-dependent equation for a particle in nucleus A is

$$i\frac{\partial}{\partial t}\phi_a = \left[-\frac{\nabla^2}{2m} + V_A(r) + V_B(r-R) + m\ddot{R}\cdot r\right]\phi_a. \tag{8}$$

The wave function in the c.m. coordinate system, or other inertial coordinate system, is related to this by a phase factor

$$\phi_a^{\text{inertial}} = \exp\left[i\boldsymbol{k}\cdot\boldsymbol{r}\right]\exp\left[-\int i\,\frac{k^2}{2m}\,\mathrm{d}t\right]\phi_a, \tag{9}$$

where $k = m\dot{R}$. We shall consider mainly Coulomb trajectories. The Coulomb potential is smooth and when expanded in multipoles, the average dipole field would just cancel the acceleration term in eq. (8).

2.2. ORTHOGONALITY

The solution to eqs. (2) and (4) can be expressed formally as

$$\phi_a = U(t)\phi_a^{(0)}, \tag{10}$$

where $U(t)$ is the evolution operator associated with eq. (8). Since U is independent of a this shows directly that

$$\langle\phi_a|\phi_{a'}\rangle = \langle\phi_a^{(0)}|\phi_{a'}^{(0)}\rangle. \tag{11}$$

So, if one starts with an orthonormal set of functions $\phi_c^{(0)}$, the set of functions ϕ_c is also orthonormal at each instant, *even if c and c' were initially in different nuclei.* This is a very important property which allows us to ignore the Pauli principle. Without such a relation it would not have been possible to obtain meaningful results with our calculations. In practice, it means that the scalar product $\langle\phi_c|\phi_{c'}\rangle$ is conserved. So if we start the cluster A and B sufficiently far apart so $\langle\phi_c^{(0)}|\phi_{c'}^{(0)}\rangle \approx 0$ for c and c' belonging to different nuclei, we can indeed use the shell-model wave functions in each nucleus as a starting point.

2.3. ENERGY

The single-particle model is not suitable for calculation of total energies. However, excitation energies as determined from single-particle energies in the potential well agree quite well with Hartree-Fock calculations. Thus, we can examine the asymptotic wave functions after the collision, and determine the inelasticity of the collision by the change in single-particle energies,

$$\Delta E = \sum_c \left(\langle\phi_c|h|\phi_c\rangle - \langle\phi_c^{(0)}|h\phi|_c^{(0)}\rangle\right). \tag{12}$$

Of course the energy must be measured in an inertial frame. This is then

$$E_c = \langle\phi|h|\phi_c\rangle = \left(\langle h_c\rangle + \boldsymbol{p}_c\cdot\boldsymbol{v} + \tfrac{1}{2}mv^2\right). \tag{13}$$

Here p_c is the expectation of the momentum of the particle in the frame A, and v is

the velocity of the inertial frame with respect to frame A. This inelasticity must imply that energy is extracted from the collective motion of the two centers. This will happen automatically if the appropriate prescription is used for the coordinates R_A and R_B.

For example, with the formulation of the problem given in the appendix, the classical trajectory of the ions is determined by the self-consistent potential defined in the appendix:

$$V(R) = \mathrm{Tr}_c(h_c\rho_c). \tag{14}$$

It is useful to define the change in the density from its initial value

$$\delta\rho_c = \rho_c - \rho_c^{(0)}. \tag{15}$$

Then this potential becomes a sum of two terms,

$$V(R) = V^{(0)}(R) + \mathrm{Tr}_c(h_c\delta\rho_c). \tag{16}$$

The first term is the potential in the sudden approximation, also known as the folding potential. It is a coherent energy which produced a conservative force. The second term, giving corrections due to single-particle motion during the collision, contains a coherent part, but gives also rise to inelastic effects. Using eq. (A.15), the rate of energy change may be expressed as

$$\frac{\mathrm{d}E}{\mathrm{d}t} = -v\cdot\nabla_R\int V_c(R-r)\delta\rho_c(r)\mathrm{d}^3r, \tag{17}$$

provided $V^{(0)}(R)$ is treated as a scattering potential in the equation of motion for R. The fact that energy is lost from collisions is apparent from the behavior of $\delta\rho_c$: it will grow during the course of the collision, and will have high overlap with the potential well of the collision partner. This means that there will be a gain of energy in the initial part of the collision, which is more than balanced by the energy loss in the final stages.

We also note with this formulation that only the higher orbits, for which $\delta\rho$ differs significantly from zero, need be considered explicitly during the collision. The other orbits only contribute to the coherent potential, which can be taken empirically in any case.

The degree of inelasticity will depend greatly on how close the collision is. When dealing with close collisions well above the Coulomb barrier, a typical time for the variation of the potential is

$$T_1 \approx a/v_c, \tag{18}$$

where v_r is the speed of the ions along the line joining their centers and a the surface thinkness. This time is quite short. Even when the radial kinetic energy is only 1 MeV per particle, the interaction occurs within a time of the order of 10 fm/c. This is to be

compared to a typical single-particle time

$$T_{\text{s.p.}} \approx \frac{2R}{v_F} \approx \frac{8\ \text{fm}}{0.3c} \approx 25\ \text{fm}/c, \tag{19}$$

where R is the nuclear radius and v_F the Fermi velocity. Thus such a collision is non-adiabatic. A similar estimate was made by Broglia and Winther [3]).

For grazing collisions and collisions near the barrier, the collision time interval is much longer. Near the classical turning point, the distance between centers will vary quadratically,

$$R(t) = R_0 + \alpha t^2. \tag{20}$$

For head-on collisions, the parameter α can be estimated from the Coulomb force as

$$\alpha = v_\infty / 4D, \tag{21}$$

where D is the distance of closest approach and v_∞ is the incident velocity of the projectile. Values for α in typical collision geometries are given in table 1. The effects of the collision in the peripheral region will depend exponentially on the distance between centers, $e^{-\kappa R}$, where κ is the rate of fall-off of the density or the potential, and is about 1–2 fm^{-1}. Then the effective length of the collision is given by

$$\int e^{-\kappa\alpha t^2} dt = \sqrt{\pi/\kappa\alpha}. \tag{22}$$

The collision times obtained from eq. (22) are of the order of 100 fm/c. The energy associated with this time is 2 MeV. Since this energy is smaller than the relevant single-particle energy spacings, the adiabatic picture is likely to be quite suitable for

TABLE 1
Collision duration parameter for $^{18}O + ^{120}Sn$

E_{lab}	D (fm)	α (Coulomb) (10^{-4} fm/(fm/c)^2)	α (Coulomb+nuclear)
60 MeV	14	1.6	1.6
	12	1.7	1.3
100 MeV	12	3.5	
	10.9	3.9	penetrates

D is the distance of closest approach.

peripheral collisions despite the exponential behaviour ($e^{-\kappa R}$) of the form factors. This is due to the properties of the classical trajectory near the turning point where the particle spends a rather long time without any change in the radial coordinate (the radial velocity vanishes).

2.4. PERTURBATION THEORY

In perturbation theory we start from the solution of eq. (8) for nucleons in nucleus A, and assume that v_B is small. Then wave function evolves in time according to

$$\Phi = e^{-ih_A t}\left(1+\int dt\, e^{ih_A t} V_B e^{-ih_A t}\right)\Phi^{(0)}, \tag{23a}$$

that is

$$\phi(r,t) = e^{-iE_a t}\phi_a^{(0)}(r) + \sum_{a'} c_{aa'}(t) e^{-iE_{a'}t}\phi_{a'}^{(0)}(r), \tag{23b}$$

with the admixture amplitudes $c_{aa'}(t)$ given by

$$c_{aa'}(t) = -i\int_{-\infty}^{t} d\tau e^{-i\omega_{aa'}\tau}\int d^3r(\phi_{a'}^{(0)}(r))^* V_B(r-R(\tau))\phi_a^{(0)}(r), \tag{24}$$

$$\omega_{aa'} = E_a - E_{a'}. \tag{25}$$

The states a' are a complete set of states in the basis including state a; thus eq. (24) is directly applicable to the inelastic excitations in nucleus A, due to the potential V_B. A similar relation can be derived for the transfer reaction using the distorted wave Born approximation, which is based on a standard formula for the transition amplitude [4]). The transfer amplitude is

$$c_{ab}(t) = -i\int_{-\infty}^{t} d\tau e^{i\omega_{ab}\tau}\int d^3r\phi_b^{*(0)}(r-R(\tau))V_B(r-R(\tau))\phi_a^{(0)}(r), \tag{26}$$

with ϕ_b an eigenstate of the potential well V_B.

We shall compare amplitudes obtained from eqs. (13) and (15) with the exact results of the model, namely

$$c_{ca}^{\text{exact}}(t) = \langle\phi_c^{(0)}|\phi_a(r,t)\rangle, \tag{27}$$

with ϕ_a the solution of the time-dependent Schrödinger equation, eq. (6).

Note that since there in general some energy loss along the trajectory $R(t)$, time reversal would not simply imply, in (26) besides changing V_B into V_A, to have the particle run backwards on the same trajectory, although our equations are invariant under the time reversal transformation. A meaningful comparison of (26) and (27) can only be done when the trajectory in (26) is chosen to be the *same* as the one used for (27). This is the recipe that replaces the usual optical potential used for DWBA calculation the relation (26) in the result of perturbation theory (i.e. assuming V_B weak for the specific transition $a \to b$) within our model. It is the result that should be checked against (27) in order to asses the validity of the DWBA theory. Eq. (27) is equivalent to a multi-channel calculations where an infinite number of channels are taken into account. This is specially important in case all the initial orbitals are spatially deformed due to a flow of matter from one ion towards the other, before transfer occurs.

A final important remark has to be made about recoil effects, which appear in standard distorted-wave Born treatments of transfer reactions. The recoil calculation

is a simultaneous integration over projectile coordinate and transferred particle coordinate, which is necessary in the DWBA formalism to properly account for momentum mismatches in the transfer of the particle from one nuceus to another. In our model, we do not explicitly identify the c.m. coordinate of the projectiles, and momentum mismatches to particular states appear automatically in the amplitudes of the wave function propagated to these states.

The states which receive large transfer amplitudes in our treatment will be well-matched in the DWBA theory when recoil is included. States receiving small amplitudes are not well described in our model, since the collective motion of the c.m. is governed by the average energy and mass transfer. However, one might argue that DWBA also does poorly on the weak amplitudes, since multistep reactions then become competitive.

3. Practical calculation

3.1. PARTIAL WAVE EXPANSION

The wave function is expressed in spherical coordinates with a partial wave expansion,

$$\psi(r, t) = \sum_{lm} Y_m^l(\hat{r}) r \phi_{lm}(r, t). \tag{28}$$

In the following, we shall assume that ϕ_a is expanded in partial waves around the center of A, and ϕ_b around the center of B. It might in some cases be as simple to expand both around a common origin. Eq. (2) can then be written

$$i \frac{\partial}{\partial t} \phi_{lm}(r) = \left[\frac{p^2}{2m} + V(r) \right] \phi_{lm}(r) + \sum_{l'm'} V_{mm'}^{ll'}(r, R(t)) \phi_{l'm'}(r), \tag{29}$$

$$V_{mm'}^{ll'}(r, R(t)) = \sum_{LM} V_{LM}(r, R(t)) G_{mMm'}^{lLl'}, \tag{30}$$

where the geometric coefficient G is

$$G_{mMm'}^{lLl'} = (LMl'm'|lm)(L0l'0|l0)\sqrt{(2L+1)(2L'+1)/4\pi(2l+1)}. \tag{31}$$

In order to describe a particle at the Fermi surface in the nucleus B, the number of partial waves to be retained is roughly

$$n \approx k_F(R_A + 2R_B), \tag{32}$$

i.e. it is roughly three times the number of partial waves needed in order to describe the ground state of A.

From the spatial distribution of the spherical harmonics $Y_{lm}(\hat{r})$ it can be inferred that the maximum contribution comes from $m \approx 0$ when the quantization axis is chosen along the line joining the A and B centers at the distance of closest approach.

In the calculation below, we limit ourselves to $m = 0$ and neglect $L \geqq 10$. According to the above considerations, this implies that we could only describe the Fermi surface to a distance of 7.5 fm from the center of nucleus A. However, the momentum

of transferred particles is primarily in the radial direction, so we actually do not need to include wave functions with large tangential momentum in our space.

3.2. INTEGRATION SCHEME

We represent the radial wave function on a mesh in coordinate space. Choosing mesh size h, the radial kinetic operator is taken as

$$t^{\text{num}} = \frac{1}{2mh^2}[\phi(r+h)-2\phi(r)+\phi(r-h)]. \tag{33}$$

Koonin [1]) uses $h = 0.4$ fm, which causes an error of 2 % in the energy at the Fermi momentum. We do not consider this to be a serious error, and use the same size mesh. Then with seventy radial points our space is a sphere of radius 28 fm. Our single-particle Hamiltonian H^{num} may be considered as a matrix operator which acts on a 700-component vector.

An excellent algorithm for time integration in one dimension is

$$\phi(t+\tau) = (1+\tfrac{1}{2}H^{\text{num}}\tau)^{-1}(1-\tfrac{1}{2}iH^{\text{num}}\tau)\phi(t). \tag{34}$$

This algorithm preserves normalization and conserves energy (of H^{num}). It is easy to do in one dimension because H^{num} is a tridiagonal matrix and the inversion can be done quickly. With the coupled partial wave equations, this is no longer true. It is out of the question to invert large matrices at each time step. One algorithm which works well is

$$\phi(Lr, t+\tau) = \sum_{L'r'} O(Lr, L'r')\phi(L'r', t), \tag{35}$$

with

$$O(Lr, L'r') = (1+\tfrac{1}{2}iH^{\text{rad}}\tau)^{-1}(1-\tfrac{1}{2}iH^{\text{rad}}\tau)\,\frac{(1+iV^{LL'}(r')\tau)}{\sqrt{1+\sum_{L'L''}(\phi(L'r')V^{L'L''}(r')\tau\phi(L'')}}.$$

The radial Hamiltonian H^{rad} of course contains the radial kinetic energy. We also include in it the potential field along the line of centers. This potential field is then subtracted out of $V^{LL'}(r)$. The algorithm (35) preserves normalization in a way which satisfies the radial equation of continuity. We expect therefore, that mass flux is adequately described.

An alternate method, which gives essentially equivalent results is

$$O(Lr; L'r') = (1+\tfrac{1}{2}iH^{\text{rad}}\tau)^{-1}(1-\tfrac{1}{2}iH^{\text{rad}}\tau)[(1+\tfrac{1}{2}iV\tau)^{-1}(1-\tfrac{1}{2}iV\tau)]^{LL'}. \tag{36}$$

Now H^{rad} is the sum of the kinetic energy operator and the potential of the initial nucleus. The non-diagonal part of the Hamiltonian in the partial wave representation is included in V. This algorithm does not conserve the norm. However, the flux lost has a numerical significance: it is the flux gone into the partial waves which were not included in the calculation.

Most of our calculations were done with a time step of 1 fm/c. Then 200 to 300 steps are needed to trace out a collision for the period where the nuclei are within a couple of fm of the closest approach point.

With the MSU Cyclotron computer (8 μs multiplication time) the calculation takes about 30 min per orbit. At the Saclay 7600 CDC, the calculation time is about sixty times less. Most of the time is spent computing $V^{LL'}(r)$. If the computer is large enough to store this array, all the single-particle states can be integrated simultaneously for a great saving in computer time.

The main check on the accuracy of the algorithm is to decrease the time step and examine the stability of the results. In fact, with the 1 fm/c time step transfer probabilities can be in error by as much as 3 % of their value, for the close collisions. Another more stringent check is whether the instantaneous Hamiltonian is conserved, i.e.

$$\langle(t+\tau)|H^{\text{num}}(t)|\phi(t+\tau)\rangle \stackrel{?}{=} \langle\phi(t)|H^{\text{num}}(t)|\phi(t)\rangle. \tag{37}$$

We found that a time step of 1 fm/c conserves the instantaneous Hamiltonian to about a tenth of an MeV over the course of the collision. This error does not affect our calculation of the inelasticity of the collision, because we calculate the change in the expectation of H as

$$\frac{\mathrm{d}\langle H\rangle}{\mathrm{d}t} = \langle\phi|\frac{\mathrm{d}V}{\mathrm{d}t}|\phi\rangle.$$

Another check we made is to calculate the evolution of an arbitrary wave function in an oscillator well. The wave function returns to its initial form in a time $2\pi/\omega$. This test proved to be the least stringent of all, probably because the smoothness of the oscillator well promotes convergence at large time steps.

3.3. EIGENSTATES

To examine the structure of the final state in terms of shell excitations, and transfers to specific orbits, we need to find the eigenstates of H^{num}. We use an iterative procedure starting with a trial wave function. We operate on the trial wave function with $O(r, r')$ and construct a vector from $\mathcal{O}\phi$ orthogonal to ϕ. The Hamiltonian H^{num} is diagonalized in the 2×2 basis defined by these two vectors. The lower eigenvector is the new trial vector. It would be more straightforward to use H^{num} instead of $\mathcal{O}$ to define the new vector. However, H^{num} acting on ϕ accentuates the high energy components, and convergence is much slower.

The above proceedure converges to the ground-state energy to within 0.01 MeV in twenty iterations, starting from a trial wave function proportional to the potential. Other states besides the ground state are obtained in the same way, except that trial vectors are orthogonalized to the previously obtained states at each iteration.

In table 2 we list the bound states obtained for the well of Sn at 14 fm from the origin of the coordinate system. The number of internal nodes in the wave function in the angular and radial directions (with respect to the coordinate system origin, not

TABLE 2
Eigenstates of Sn well at 14 fm from origin

Level number	Energy	Radial nodes	Angular nodes	Spherical state	$E^{\text{spherical}}$
1	−43.6	0	0	0s	−43.8
2	−37.4	1	0	$0p_0$	−38.0
3	−29.3	2	0	$(0d+1s)_0$	−29.1, −31.1
4	−19.8	3	0	$(0f+1p)_0$	−20.5, −23.4
5	−12	0	1	$0p_1$	−38.0
6	−10.2	4	0	$(0g+1d+2s)_0$	−10.8, −11.6, −14
7	− 4	1	1	$0d_1$	−31.1
8	− 0.33	5	0	$(0h+1f+2p)_0$	− 2.6, −3.1, −5.9

the Sn center of the Sn well) is determined, and from this one can associate a spherical wave function, and corresponding eigenenergy.

We see that the energies of wave functions with no angular nodes are reasonably given, except for the highest state which is off by several MeV. However, the energies of states with angular nodes are quite far off. This indicates the insufficiency of the cut-off in angular momentum of $L = 9$.

4. Results

4.1. INTRODUCTION

We consider as a model system the collision of ^{18}O on ^{120}Sn, because this has been thoroughly studied experimentally [6,11]) and theoretically in DWBA [5]). The subjects we investigate are the validity of perturbation theory in the peripheral region, the dynamics of mass flow at the point of contact, and the inelasticity of the collision. For most cases we used a pure Coulomb trajectory for the classical motion of the ions. At the energies we consider the nuclear potential plays a negligible role when the distance of closest approach is greater than 11.5 fm. The single-particle potentials appearing in eq. (6) will be taken as Woods-Saxon wells with the standard geometry $r_0 = 1.25$, $a = 0.65$. The depth of the Sn well is 50 MeV. This is increased to 57 MeV for the ^{18}O to bind the d-orbit by 5.5 MeV.

4.2. COMPARISON WITH PERTURBATION THEORY

The DWBA theory used for peripheral reactions enjoys quantitative success on the magnitudes of inelastic scattering and single-particle transfer reactions. Two-particle transfer reactions are systematically underpredicted by a factor of 5–10 [ref. [9])], although in some cases multistep reaction mechanisms can improve the agreement. In some cases the reaction is sensitive to relative phases among the two-particle transfer amplitudes [7]).

The simplest question that can be asked in a single-particle model is whether it is more likely to inelastically excite the particle in the same nucleus or whether a transfer

to the other nucleus is more likely to take place. In the semiclassical Born theory, eqs. (24) or (26) the question reduces to whether $V_B\phi_a$ has a larger overlap with orbits in nucleus A or in nucleus B. For orbits at the Fermi level, the transfer amplitude is larger. Let us consider specifically the d-orbit in ^{18}O. Choosing an oxygen well that binds this orbit by 5.5 MeV, we examine the time-dependent behavior of the wave function as the potential well of the Sn nucleus moves by on a Coulomb trajectory. In table 3 we compare the probabilities for transfer and for inelastic excitation. The transfer probability was obtained by finding the change in probability at radius greater than 6 fm from the center of the oxygen well. The excitation probability is determined by taking of overlap of the final state with the other bound orbits of oxygen, namely 0s, 0p and 1s. The transfer probability overwhelmingly dominates as might be expected. The excitation probability is almot completely to the 1s orbit, which lies within 0.8 MeV of the 0d orbit. We consider now the total inelastic or transfer probability P_a for a nucleon initially in state a. Whereas the transfer probability from a given state a to a given state b is essentially determined by the Q-value, the total transfer is not, since one sums up all final states. It is basically governed by the height of the barrier built up by V_A+V_B between the two nuclei. If the top of this barrier is higher than the binding energy of the initial state a, transfer is small, when on the other hand the barrier is low enough to allow the particle in state a to propagate classically into the other nucleus, transfer is larger. Another factor, is the ratio of the volumes of nuclei A and B. Transfer is easier from the smaller towards the larger nucleus. For instance, in the case of a p-wave proton, shown in table 4, the long range of the Coulomb interaction increases the inelastic strength so that it became comparable to the transfer strength. We also note that proton transfer is inhibited compared to neutron transfer, as would be expected from the Coulomb barrier of V_A+V_B between the clusters.

In the last column of table 3, labelled $P_{L'}$, we tabulate the amount of flux lost to higher partial waves with the algorithm, eq. (36). The number is quite large. However, it does not directly indicate the probability in the higher partial waves, since we have not allowed for a flux in the reverse direction.

In tables 5 and 6 we display the amplitudes to specific states, including the diagonal

TABLE 3

Evolution of d_0 orbit in 61 MeV ^{18}O on ^{120}Sn

D	P_{transfer}	$P_{\text{excitation}}$	$P_{L'}$
12	17 %	0.7 %	25 %
13	6.3 %	0.1 %	10 %
14	1.6 %		3 %

Probabilities for transfer, inelastic excitation, and flux to partial waves higher than nine are shown.

TABLE 4
Evolution of p-orbits in ^{16}O, including the Coulomb fields

		P_t	P_{ex}
neutron	SE	4 %	1×10^{-3} %
	BA	5×10^{-4}	4×10^{-4}
proton	SE	2	2
	BA	0.07	1

The Schrödinger results (SE) are compared with the Born approximation (BA) for the collision with ^{120}Sn at $E = 60$ MeV and $D = 11$ fm.

TABLE 5
Inelastic amplitudes

	$v_{ij} = \eta e^{i\theta}$ d → d		$D = 12$ fm d → 1s	
	SE	BA	SE	BA
η	0.906	1	0.10	0.18
θ	5°	11°	163°	110°

TABLE 6
Particle transfer amplitudes

R		Orbit in Sn (6)	(7)	(8)
12	SE	0.29	0.06	0.11
	BA	0.14	0.11	0.10
14	SE	0.056	0.049	0.053
	BA	0.045	0.036	0.040

d → d amplitudes calculated from the formula (26) and (27), using the exponential amplitudes (22). The potential matrix element is given by

$$\int d^3r \phi_c^{*(0)}(r) V(r+R) \phi_a^{(0)}(r) \approx V_0 e^{-\kappa(R-D)}.$$

The reaction amplitudes are then expressed analytically as

$$c_{ca} = V_0 \sqrt{\pi/\kappa\alpha} \exp\left[-\omega_{ca}^2/4\kappa\alpha\right].$$

The parameter V_0 is determined from actual overlap integral at D. The parameter κ is estimated from the integral at another point or the rate of decay of the wave functions. These parameters are given in table 7.

The comparison of transfer amplitudes in table 6 shows rough agreement between the two theories. In the DW theory, the amplitudes to the three least bound orbits are

TABLE 7
Overlap integrals in the $^{18}O+^{118}Sn$ collision

Orbits	D	V_0 (MeV)	κ (fm^{-1})
0d, 0d	12	0.33	1.15
0d, 1s		0.27	
0d, Sn (6)	14	0.25	0.56
0d, Sn (7)		0.06	
0d, Sn (8)		0.17	

roughly comparable. This is due to a coincidence: the orbits (6) and (8) stick relatively far out in the surface, and so have a good spatial overlap, but the energy difference ω is 5 MeV which reduces the amplitude to these orbits by a substantial factor.

For the inelastic amplitude, the Born amplitude differs from the Schrödinger equation by nearly a factor of 2, but more important, the phase of the admixture is quite different from the Born phase. We believe that this phase has a physical significance. The domniant process in the reaction is transfer, and the probability density is depleted in the region of the oxygen surface near the Sn well. The phase is exactly opposite to the sudden picture, which suggests that amplitudes should be admixed to increase the density along the line of centers. The actual phase in fact decreases the probability in the oxygen surface near the Sn well.

Let us now concentrate on total one-particle transfer, i.e. the probability that a particle, initially in a given eigenstate a of V_A is within a radius R_B+3 fm of the center of B in the final stage of the collision, whatever state in B has been populated. The same calculation can be done by perturbation theory, with the same initial and final states, or using the TDSPM equations. The exact calculation agrees in magnitude with the perturbative calculation only for moderate transfer amplitudes. In cases where the strength is weak, as for example the p-wave transfer in ^{18}O, the DWBA grossly underestimates the transfer probability. This may be seen in table 4, where the difference is nearly two orders of magnitude. Also, for very large transfers, the fact that the perturbative amplitude is not normalized will make it unreliable. DWBA, mostly for two particle transfer, has been often questioned [15-17]. We find *systematically* deviations from the first order calculations although there is no obvious strongly coupled intermediate channel which would call for a second a higher order calculation with only a few additional terms in order to provide such a systematics. These deviations (in phase or in magnitude) occur whatever the strength of the process is so the magnitude of the cross section alone is not a sufficient indication for the validity of perturbation theory. The reaction time might be a useful criterium, but for $^{18}O+^{118}Sn$ at 60 MeV (near the Coulomb barrier) or at 100 MeV (well above with about half the reaction time) the same qualitative features can be observed in the calculation.

4.3. COMPARISON WITH EXPERIMENT

Let us now try to make contact with experiment. According to Henning *et al.* [6], inelastic scattering is more important than transfer for $^{18}O+Sn$ in peripheral col-

lisions. We have omitted from our treatment so far the complications of the wave function being more complex than a single Slater determinant. Inelasticity can result simply from the collision's destruction of the phase relation between components of the ground-state wave function, without these necessarily being in the single-particle orbits. Also, collective effects such as core polarization have been completely neglected. Some additional transfer or inelastic excitation might also arise from the $m \neq 0$ orbitals whose contribution was neglected here.

Schematically, an account of the shell structure of ^{18}O can be made using a linear combination of the five m-states for the d-orbits:

$$\psi = \sqrt{\tfrac{1}{5}} \sum_m \phi_{\mathrm{d}m}(1)\phi_{\mathrm{d}-m}(2)\pi\phi_a. \tag{38}$$

In the coordinate system based on the line of centers at the point of closest approach, the main effect of the collision is on the d_0 orbit. The final state is then roughly

$$\psi' = \sqrt{\tfrac{1}{5}}(\eta^2 \mathrm{e}^{2i\theta}\phi_{\mathrm{d}0}\phi_{\mathrm{d}0} + \sqrt{\tfrac{1}{5}} \sum_{m\neq 0} \phi_{\mathrm{d}m}\phi_{\mathrm{d}-m})\pi\phi_a. \tag{39}$$

where $\eta \mathrm{e}^{i\phi}$ is the amplitude of d_0 in the final state. The elastic scattering amplitude is the overlap of initial and final states,

$$\langle\psi'|\psi\rangle = \tfrac{1}{5}(4+\eta^2\mathrm{e}^{2i\phi}), \tag{40}$$

$$P_{\mathrm{elastic}} = \langle\psi'|\psi\rangle^2 = \tfrac{1}{25}(16+8\eta^2\cos 2\phi+\eta^4). \tag{41}$$

The transfer probabilities are conveniently expressed in terms of the probability for transfer of the d_0 particle, P_{d}. The two-particle transfer probability is

$$P_{2\mathrm{p}} = \tfrac{1}{5}P_{\mathrm{d}}^2. \tag{42}$$

The one-particle transfer probability is

$$P_{1\mathrm{p}} = \tfrac{1}{5}2P_{\mathrm{d}}(1-P_{\mathrm{d}}). \tag{43}$$

In figs. 1 and 2 we compare the one- and two-particle transfer with the experimental results of Henning *et al.* [6]). These authors quote their results in terms of the distance of closest approach for Coulomb trajectories. The calculated curves are also for Coulomb trajectories. Inclusion of an ion ion potential in the trajectory changes the results negligibly, since the strong absorption radius is smaller, than 12 fm [ref. [5])]. The theoretical one-particle transfer is somewhat too high, but the slope matches experiment. The slope of the two-particle transfer is roughly twice the one-particle transfer (note the difference in scales in figs. 1 and 2) but the theoretical magnitude is too low by a factor of 5. Additional correlations, besides what is included in the $(\mathrm{d}^2)^0$ wave function, will increase the two-particle transfer. Including the $(1\mathrm{s})^2$ configuration has a dramatic effect. Its transfer probability of the 1s is nearly the same as for

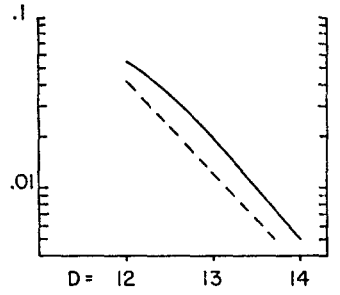

Fig. 1. Probability for one-particle transfer, ^{118}Sn(^{18}O, ^{17}O), at 60 MeV. The probability is plotted as a function of the distance of closest approach for Coulomb trajectories. The solid line is theory with eq. (40) and the dashed line is deduced from fig. 1 of ref. [6]).

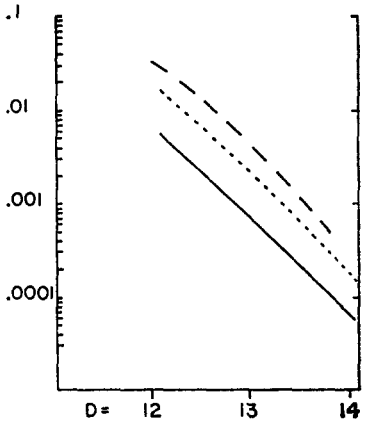

Fig. 2. Two-particle transfer probability, ^{118}Sn(^{18}O, ^{16}O) at 60 MeV. Note the compressed scale on the ordinate. Theory is the solid line from eq. (40), and the short-dashed line using the wave function of eq. (42).

the d_0, and amplitude is substantial in typical shell-model wave functions. Using the wave function [13])

$$\psi = 0.88(d^2)^{L=0}+0.32(1s^2)^{L=0}+0.35(d^2)^{L=1}, \tag{44}$$

the cross section is increased by a factor of 3.

This is shown as the short-dashed line in fig. 2. The two-particle transfer probability is now close to experiment. However, it should be noted that if the theory were modified to get agreement for the one-particle transfer, the two-particle transfer would be substantially reduced. This is to be compared with the results of DWBA theory which reproduce one-particle transfer, but have too small cross sections for two-particle transfer, typically by a factor of five [9]).

We compute the inelastic excitation cross section as

$$P_{\text{inelastic}} = 1-P_{\text{elastic}}-P_{1p}-P_{2p}. \tag{45}$$

This only amounts to 1.5 % at $D = 12$ fm. The experiment greatly exceeds the theory, but this is to be expected: core polarization effects will enhance the $0^+ \rightarrow 2^+$ transition in ^{18}O by at least a factor of 4, and excitation of the Sn nucleus has been omitted from the theory. When the collision is between closed shell nuclei, the single-particle model prediction of domination by transfer ought to be borne out. In fact, Henning *et al.* [6]) report that transfer exceeds inelastic in the case of ^{16}O on ^{48}Ca.

Experimentally the phase of the inelastic amplitudes can be found from Coulomb-nuclear interference. The $d \rightarrow 1s$ transition in ^{17}O, and the $0^+ \rightarrow 2^+$ transition in ^{18}O appear to have anomalous phases [10,11]). In fact, the direction of phase change

needed in ref. [11]) agrees with the sort of deviation we find for the d → 1s transition. This is certainly suggestive that transfer-dominated single-particle dynamics may influence the inelastic excitations.

4.3. MASS FLOW

A hydrodynamic description is desired for close collisions between nuclei, because the description in terms of nucleon coordinates seems inefficient. Hydrodynamics is based on the equation of continuity and a dynamic equation relating the change of momentum density to the local state of the medium. Both the equation of continuity and a dynamic equation can be derived from the single-particle model; the dynamic equation has the form

$$\langle \dot{P}_\mu \rangle = \nabla_\nu T_{\mu\nu}, \tag{46}$$

where the stress tensor $T_{\mu\nu}$ depends on the potential and derivatives of the wave function. Because of this nonlocality, it is not easy to derive hydrodynamic approximations useful in the surface region. Qualitatively the collision ought to behave as follows. Initially, the nuclei are in equilibrium so that the left-hand side of eq. (46) vanishes. When the other well comes by, there is a force $-\nabla V_B$, so the momentum of the nucleons is determined by

$$\langle \dot{\boldsymbol{P}} \rangle = -\nabla V_B. \tag{47}$$

Nucleon density moves into the other nucleus, stretching out the wave functions. If changes in the stress tensor due to alteration of the wave function could be neglected, the velocity field would approach asymptotically the value

$$v = \sqrt{-2V_B/m}. \tag{48}$$

In fig. 3 we have plotted the results of the Schrödinger equation for the velocity of an ^{18}O d-particle along the line of centers computed as

$$v(r) = \left\langle \frac{\hbar \nabla}{im} \right\rangle_r.$$

The collision is for 60 MeV Coulomb trajectory of ^{18}O on ^{120}Sn, with a distance of closest approach of 12 fm. The integration is started when the ions have a separation of 13.7 fm. Initially, the velocity field agrees well with eq. (47), which is shown by the comparison of the actual velocity (lowest solid curve) with eq. (47) (dashed curve) at 2 fm/c after the start of the integration of the Schrödinger equation. The other two solid curves are for $T = 30$ and 90 fm/c. We see that the wave function that penetrates within the Sn well does have a velocity field approaching eq. (48). However, in the region between the oxygen and Sn nucleus, the actual velocity only reaches half this limit.

In fig. 4 we examine the velocity in the neck region between the two nuclei, i.e. at the point midway between the edges of the O and Sn wells. The velocities for both the

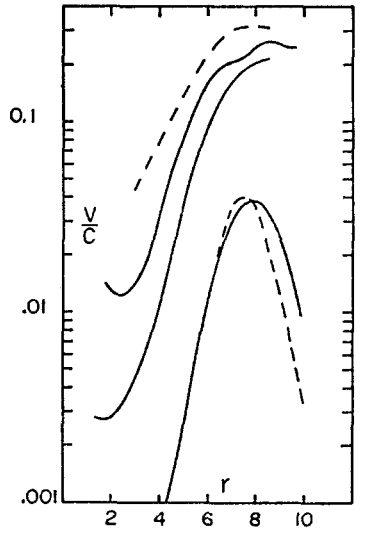

Fig. 3. Velocity of ^{18}O d-particle during a collision with ^{120}Sn, plotted along the line of centers between the two ions. The solid curves show the velocities for different times (2.30 and 90 fm/c respectively from the bottom to the top). The lower dashed curve is from eq. (44) and the upper dashed curve is from eq. (45).

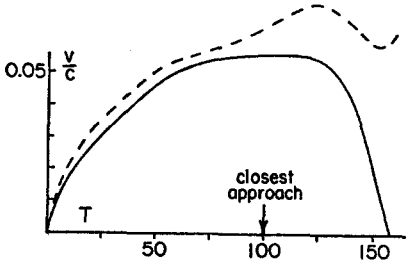

Fig. 4. Velocity of ^{18}O d-particle (solid) and 1s particle (dashed) at the point midway between the surfaces of the colliding nuclei.

0d and 1s particles are plotted as a functon of time. We see that there is a substantial time when the velocity field is essentially constant. A plausible hypothesis is that the entire flow is governed by leaking through the neck region. All the kinetic energy in the neck region should then be attributable to the coherent velocity field. If conditions are adiabatic, the particle has the same energy in the neck region as it had initially. Thus, if the potential in the neck region is V_n, the velocity would be

$$v = \sqrt{2(\varepsilon - V_n)/m}. \tag{49}$$

This idea does not work out quantitatively, either. Eq. (49) predicts a velocity of $0.1c$ at the distance of closest approach, a factor of two larger than the actual rate.

At times somewhat later than the closest approach point, the reflection of the nucleon wave function from the farther edge of the Sn well causes the velocity field in the

Sn well to become confused. This also gives rise to large fluctuations in the neck region past $T = 150$.

To summarize, the simple-minded classical description of mass flow does not stand up a quantitative test. Nevertheless, the qualitative agreement is quite impressive and extremely encouraging for a more complete hydrodynamical description of the phenomenon.

4.5. OPTICAL POTENTIAL

It should be possible to calculate phase changes associated with elastic scattering, i.e. optical potentials in the time-dependent Schrödinger equation model. We will consider a collision energy of 100 MeV, with a Coulomb trajectory that reaches $D =$ 10.9 fm separation. This still corresponds to rather peripheral collisions.

For calculating elastic scattering, we must take the overlap of the wave functions in the final state with the ground-state eigenstates, and utilize the phase information obtained. The phase is obtained in the sudden approximation by assuming that the single-particle wave functions remain in the eigenstates of the individual wells at each point of the trajectory. Then the optical potential can be defined,

$$V_{\mathrm{op}} = \sum_a \int |\phi_a^{(0)}|^2 V_{\mathrm{B}} \mathrm{d}^3 r, \tag{50}$$

and the phase is $\int \mathrm{d}\tau V_{\mathrm{op}}(\tau)$. With the TDSE, we allow the single-particle wave functions to evolve according to eq. (6), but determine the elastic phase by projecting the wave function on $\phi_a^{(0)}$. In table 8 we display the phase changes predicted by these two methods, and compare with the optical model phase change along the Coulomb orbit.

TABLE 8

Elastic phase ($j \to j$) in close collision: $E_{\mathrm{in}} = 100$ MeV; $D = 10.9$ Coulomb trajectory

	Sudden approx.	$\mathrm{Arg}\langle\phi_j^{(0)}\|\phi_j\rangle$
s → s	2.9°	2.6°
p → p	13.3°	14.5°

Total phase change with four particles in each orbit is 68.4°; from phase change in sudden approximation 64.4°; from phase change of system with phenomenological optical potential 54°.

The two methods give very similar results for the s- and p-orbits. Thus the sudden approximation is quite accurate. This is somewhat surprising, because the nondiagonal changes in the wave function are large compared with the elastic phase change. Nearly 20 % of the p-wave is transferred to the other well, but the phase change is only 13.5°.

The last row of table 8 shows the phase change along the trajectory induced by the phenomenological optical potential of ref. [5]) ($V = 40$ MeV, $r_0 = 1.31$ fm, and $a =$ 0.45 fm). This is smaller than the phase in the single-particle models, especially con-

sidering that we have not included contributions from $m \neq 0$ orbits. Satchler has compared the systematics of optical potentials with the sudden approximation [8]), finding that phenomenological potentials are typically a factor of two smaller. Our results are in the same direction, and matters are not improved by going beyond the sudden approximation to the actual wave functions which satisfy the time-dependent Schrödinger equation.

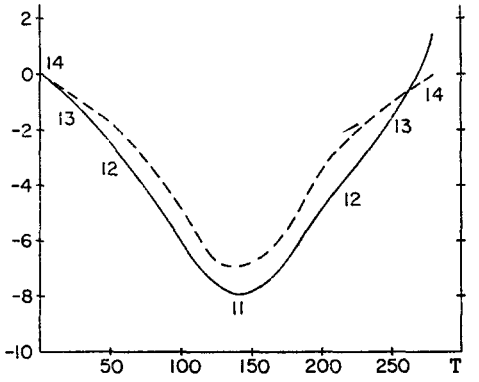

Fig. 5. Change in single-particle energy for a collision of ^{18}O on ^{120}Sn at 60 MeV. The energy in MeV for the combined systems is plotted versus time in fm/c. The closest approach is indicated by an arrow, and the distance between ions is shown along the curves.

Finally, we examine the inelasticity of the collisions, calculating the total single-particle energy as a function of time. The results for the 60 MeV collision at $D = 11$ fm is plotted in fig. 5. As the nuclei approach, the energy becomes negative. This is to be expected, since the energy can be calculated as

$$\frac{\mathrm{d}E}{\mathrm{d}t} = \sum_i \langle \phi_i | \frac{\mathrm{d}H}{\mathrm{d}t} | \phi_i \rangle = \sum_i \langle \phi_i | \frac{dV}{\mathrm{d}t} | \phi_i \rangle = \int \rho \frac{\mathrm{d}V}{\mathrm{d}t} \, \mathrm{d}^3 r,$$

which is negative for approaching wells. At the distance of closest approach it is zero, and then becomes positive. The energy returns to its initial value only much later, when the fragments are separated by 13–15 fm. We expect a net inelasticity because the density in the region between the two nuclei ought to be greater after the point of closest approach than before. In fact, the collision nearly conserves energy, showing that the adiabatic limit is most appropriate. This conclusion remains true at 100 MeV bombarding energy, and even when there is orbiting (and thus large collision time, of the order of 500 fm/c).

One should note (fig. 5) that the incident particle gains more energy where it approaches the target than predicted by the sudden approximation, i.e. using the unperturbed value $\rho^{(0)}$ of ρ for the energy change calculation. Especially, this is true for the ^{18}O d-wave contribution. It is easy to understand, since the changes in ρ as compared to $\rho^{(0)}$ are mostly due to transfer. It also is interesting to note that in case the

density matrix is calculated by perturbation theory [from eq. (28)], the net energy loss is quite large, of the order of several MeV per particle. So, one should be extremely careful when using perturbation theory.

Our model provides a unified treatment of both aspects of optical models, refraction and absorption. We find that the absorption is small compared to the elastic phase changes, in the peripheral region. This agrees with the optical model analyses of refs. [5,14]) but contradicts the assumptions of Fresnel diffraction model, as applied to heavy ion scattering.

5. Conclusion

Our initial picture of close collisions was that the strong nuclear field would greatly affect the nucleon density matrix in the region of contact of the two ions, but not affect the density matrix elsewhere. In fact we fond that the collision process was so slow that the entire density matrix is affected nearly adiabatically. The inelasticity is not very strong, either in terms of flux removal from the entrance channel, or in terms of energy loss. The observed inelasticity could be due to collective behavior, which is omitted from our model in as much as the potential wells remain spherical. Broglia *et al.* [12]) take the point of view that the collective states dominate the deep inelastic, but not the quasi-elastic reactions. The inelasticity could also be due to mixing with more complicated configurations that involve change of orbits of two particles simultaneously. One would anyway expect large inelasticity only in heavier fragments.

The single-particle dynamics may be compared with experiment by studying individual states. We found reasonable agreement for single-particle transfer and two-particle transfer, but poor agreement for inelastic excitation. The failure of the single-particle model for inelastic excitation is explicable with the neglected deformations of the potential.

This work was started at the Michigan State University. One of the authors (R.S.) would like to thank the physicists of the Cyclotron Laboratory for their hospitality.

Appendix

A.1. THE EQUATIONS OF MOTION

Let us consider two nuclear fragments A and B whose centers are respectively, at R_A and R_B. A nucleon c in one of the clusters experiences the potential

$$V_c(r_c, R) = V_A(r_c - R_A) + V_B(r_c - R_B), \tag{A.1}$$

with $R = R_B - R_A$.

We will express the Hamiltonian in terms of the cluster coordinates $r_c - R_{A(B)}$ and the conjugate momenta, p_c. The total Hamiltonian is then

$$H = \sum_c h_c + T, \tag{A.2}$$

with

$$h_c = p_c^2/2m + V_c, \quad T = P^2/2M. \tag{A.3}$$

Here P is the relative momentum of the clusters, m the nucleon mass and M their reduced mass.

The collision process is described by the time-dependent wave function ψ:

$$i\hbar \frac{\partial \psi}{\partial t} = H\psi. \tag{A.4}$$

Initially, the wave function $\psi^{(0)}$ is built up by a Slater determinant describing the nucleons in the fragments, multiplied by a wave packet describing the relative motion. Assuming ψ keeps this form at all times [this is the Hartree approximation to (A.2)] we get the equations

$$i\hbar \frac{\partial \chi(R, t)}{\partial t} = \left(\frac{P^2}{2M} + \mathrm{Tr}_c(h_c\rho_c)\right) \chi(R, t), \tag{A.5}$$

$$i\hbar \frac{\partial \phi_c}{\partial t} = \left(\frac{p_c^2}{2m} + \mathrm{Tr}_c(h_c\rho_R)\right) \phi_c, \tag{A.6}$$

with

$$\rho_c = \sum_i |\phi_i|^2, \qquad V = \sum V_c, \qquad \rho_R = |\chi(R, t)|^2.$$

The wave packet of the relative motion ρ_R is built up with the wave function χ, and the single-particle wave functions are ϕ_c. If the wave packet ρ_R is sufficiently narrow, (A.6) can be replaced by

$$i\hbar \frac{\partial \phi_c(r_c, t)}{\partial t} = \left\{\frac{p_c^2}{2m} + V_c[r_c, R(t)]\right\} \phi_c(r_c, t), \tag{A.7}$$

with $R(t)$ determined by the classical motion of a particle in the potential

$$V(R) = \mathrm{Tr}\ h_c\rho_c. \tag{A.8}$$

An overall phase exp $[i\int (p^2(t)/2M)\mathrm{d}t]$ of ϕ_c has been dropped in (A.7). Eq. (A.7) together with the equation for $R(t)$ from (A.8) are the semi-classical Hartree-Fock solutions of (A.4).

The initial conditions are given by $\phi_c(r_c, 0) = \phi_a^{(0)}(r_c - r_A)$ or $\phi_c(r_c, 0) = \phi_b^{(0)}(r_c - r_B)$ depending on which cluster the nucleon c is initially, with

$$\begin{aligned} \left(\frac{p_c^2}{2m} + V_A(r)\right) \phi_a^{(0)}(r) &= \varepsilon_a \phi_a^{(0)}(r), \\ \left(\frac{p_c^2}{2m} + V_B(r)\right) \phi_b^{(0)}(r) &= \varepsilon_b \phi_b^{(0)}(r). \end{aligned} \tag{A.9}$$

A.2. MICROSCOPIC POINT OF VIEW

Starting from an underlying Hartree-Fock theory, and a two-body potential v_{12},

the energy can be written as

$$E = \mathrm{Tr}\,(t\rho)+\tfrac{1}{2}\mathrm{Tr}\,(v_{12}\rho\rho). \tag{A.10}$$

Assuming ρ is a product of a density matrix describing the relative motion of the clusters and an internal density, i.e.

$$\rho = \rho_R\rho_c, \tag{A.11}$$

with $\rho_R(R, t)$ peaked at the classical value $R = R(t)$ we obtain, since $t = T+\sum t_c$ according to (A.3)

$$E = \tfrac{1}{2}M\dot{R}^2(t)+\mathrm{Tr}\,(t_c\rho_c)+\tfrac{1}{2}\,\mathrm{Tr}\,(v_{12}[R(t)]\rho_c\rho_c). \tag{A.12}$$

Considering the linearisation of E near the density of non-interaction clusters

$$\rho^{(0)} = \rho_R\rho_c^{(0)} = \rho_R(R, t)[\rho_A^{(0)}(r-R_A)+\rho_B^{(0)}(r-R_B)], \tag{A.13}$$

the single-particle model energy is

$$\begin{aligned} E &= \tfrac{1}{2}MR^2(t)+\mathrm{Tr}\,(t_c\rho_c^{(0)})+\tfrac{1}{2}\,\mathrm{Tr}\,v_{12}\rho_c^{(0)}\rho_c^{(0)}+\mathrm{Tr}\,(t_c\delta\rho_c)+\mathrm{Tr}\,(v_{12}\rho_c^{(0)}\delta\rho_c) \\ &= \tfrac{1}{2}MR^2(t)+\tfrac{1}{2}\,\mathrm{Tr}\,(V_A\rho_B+V_B\rho_A)+\mathrm{Tr}\,(h_c\delta\rho_c). \end{aligned} \tag{A.14}$$

In the last equation the internal energy of the clusters at time $t = 0$ has been put equal to zero.

By definition the sudden potential is

$$V^{(0)} = \tfrac{1}{2}\,\mathrm{Tr}\,(V_A\rho_B+v_B\rho_A). \tag{A.15}$$

The factor of $\frac{1}{2}$, which was not in (A.8) avoids the double counting of the two-body interaction, and the correct equation, in place of (A.8) is

$$V(R, t) = V^0(R)+\mathrm{Tr}\,(h_c\delta\rho_c). \tag{A.16}$$

Similar, the correct single-particle equations which replaces (A.5) is

$$ih\frac{\partial\chi(R, t)}{\partial t} = \left[\frac{P^2}{2M}+V^{(0)}(R)+\mathrm{Tr}\,(h_c\delta\rho_c)\right]\chi(R, t). \tag{A.17}$$

A.3. ENERGY CONSERVATION

The rate of change of energy is given by

$$\frac{\mathrm{d}E}{\mathrm{d}t} = \dot{R}[M\ddot{R}+\nabla_R V^0]+\mathrm{Tr}\,(\dot{h}_c\delta\rho_c)+\mathrm{Tr}\,(h_c\delta\dot{\rho}_c). \tag{A.18}$$

But $\mathrm{Tr}\,(h_c, \dot{\rho}_c) = 0$, since $\dot{\rho}_c = [h_c, \rho_c]$ and $\rho_c^{(0)}$ does not depend on time since the relative motion of the clusters has been extracted out, so

$$\frac{\mathrm{d}E}{\mathrm{d}t} = \dot{R}[M\ddot{R}+\nabla_R V^0+\mathrm{Tr}\,(\delta\rho_c\nabla_R v_c)] = \dot{R}[M\ddot{R}+\nabla_R V] = 0, \tag{A.19}$$

since the motion of $R(t)$ is to be calculated in the (time-dependent) potention $V(R, t)$ obtained from (A.16).

The energy less (or gain!) along the trajectory as compared to the motion in the sudden potential is

$$\frac{dE_T}{dt} = \frac{d}{dt}(\tfrac{1}{2}MR^2 + V^{(0)}). \tag{A.20}$$

It is equal to the energy gone into the intrinsic degrees of freedom

$$\frac{dE_T}{dt} = -\frac{d}{dt}\,\mathrm{Tr}\,(h_c\delta\rho_c). \tag{A.21}$$

A.4. DENSITY DEPENDENCE OF THE TWO-BODY INTERACTION

Let us indicate how eq. (A.16) would be modified when the two-body interaction depends on density. An interaction of the Skyrme type

$$v_{12}(r, r') = [\alpha + \tfrac{2}{3}\beta\rho(r)]\delta(r-r'), \tag{A.22}$$

leads to single-particle potentials for nuclei A and B of the form

$$\begin{aligned} V_A &= \alpha\rho_A^{(0)} + \beta\rho_A^{(0)^2}, \\ V_B &= \alpha\rho_B^{(0)} + \beta\rho_B^{(0)^2}. \end{aligned} \tag{A.23}$$

But, the sudden potential (A.15) is now expressed, using (A.22) with $\rho = \rho_A^{(0)} + \rho_B^{(0)}$ as

$$V^{(s)} = \tfrac{1}{2}[2\alpha\rho_A^{(0)}\rho_B^{(0)} + 2\beta\rho_A^{(0)^2}\rho_B^{(0)} + 2\beta\rho_B^{(0)}\rho_A^{(0)^2}], \tag{A.24}$$

that is

$$V^{(s)} = \tfrac{1}{2}\,\mathrm{Tr}\,(V'_A\rho_B^{(0)} + V'_B\rho_A^{(0)}), \tag{A.25}$$

with

$$\begin{aligned} V'_A &= V_A + \beta\rho_A^{(0)}\rho_B^{(0)}, \\ V'_B &= V_B + \beta\rho_A^{(0)}\rho_B^{(0)}, \end{aligned} \tag{A.26}$$

i.e. one has to add a repulsive counter term to the single-particle potentials.

Similarly, the linear term in (A.14) has to be replaced by

$$\mathrm{tr}\,(h'_c\delta\rho_c), \tag{A.27}$$

with $h'_c = t_c + v'$.

The densities $\rho_A^{(0)}$ and $\rho_B^{(0)}$ can, in addition be calculated as a function of V_A and V_B taken from (A.23), so the effective single-particle potentials V'_A and V'_B taking the density dependence of the two-body interaction can be written in terms of the same

potentials V_A and V_B for the separated ions:

$$V'_A = V_A + \frac{1}{\gamma}(1-\sqrt{1-\gamma V_A})(1-\sqrt{1-\gamma V_B}),$$

$$V'_B = V_B + \frac{1}{\gamma}(1-\sqrt{1-\gamma V_A})(1-\sqrt{1-\gamma V_B}), \tag{A.28}$$

$$\gamma = 4\beta/\alpha^2.$$

From (A.26) it can be clearly seen that the counter term (A.28) weakens the single-particle potential in the region of overlap of the two clusters ($V_A V_B \neq 0$).

Eqs. (A.25), (A.27) and (A.28) can be used in order to take the density dependence of the two-body interaction into account. From standard parameters of the Skyrme interaction, one has $\gamma \approx 0.02$ MeV^{-1}.

References

1) P. Bonche, S. Koonin and J. Negele, Phys. Rev. **C13** (1976) 1226;
S. Koonin, Phys. Lett. **61B** (1976) 327;
R. Y. Cusson *et al.*, Phys. Rev. Lett. **36** (1976) 1166
2) G. Breit and M. E. Ebel, Phys. Rev. **103** (1956) 679
3) R. A. Broglia and A. Winther, Phys. Reports **4C** (1972) 154
4) N. Austern, Direct nuclear reaction theories (Wiley, NY, 1970) p. 48
5) N. K. Glendenning, Rev. Mod. Phys. **47** (1975) 659
6) W. Henning *et al.*, Phys. Lett. **58** (1975) 129
7) D. K. Scott *et al.*, Phys. Rev. Lett. **34** (1975) 895
8) G. R. Satchler, Phys. Lett. **59B** (1975) 121
9) J. Peterson *et al.*, Phys. Rev. Lett. **36** (1976) 307
10) T. Motobayashi *et al.*, Phys. Rev. Lett. **36** (1976) 390
11) K. E. Rehm, *et al.*, Phys. Rev. **C12** (1975) 1945
12) R. A. Broglia, C. H. Dasso and A. Winther, Phys. Lett. **53B** (1974) 30; **61B** (1976) 113
13) T. T. S. Kuo and G. E. Brown, Nucl Phys. **85** (1966) 40
14) J. Knoll and R. Schaeffer, Ann. of Phys. **97** (1976) 307; Phys. Reports, to be published
15) R. J. Ascuitto and N. K. Glendenning, Phys. Lett. **47B** (1973) 332
16) U. Gotz, M. Ichimura, R. A. Broglia and A. Winhter, Phys. Reports **16C** (1975) 115;
J. Bang *et al.*, Nucl. Phys. **A364** (1976) 157
17) D. K. Scott *et al.*, Phys. Rev. Lett. **34** (1975) 895;
M. E. Cobern *et al.*, Phys. Rev. **C13** (1975) 1200